Zhang *et al.*
Chinese Journal of Mechanical Engineering (2023) 36:99
https://doi.org/10.1186/s10033-023-00917-2

Chinese Journal of Mechanical Engineering

ORIGINAL ARTICLE

Open Access

Design and Research of Form Controlled Planar Folding Mechanism based on 4D Printing Technology

Wencai Zhang[1], Zhenghao Ge[1] and Duanling Li[1,2*]

Abstract

The use of non-smart materials in structural components and kinematic pairs allows for flexible assembly in practical applications and is promising for aerospace applications. However, this approach can result in a complex structure and excessive kinematic pairs, which limits its potential applications due to the difficulty in controlling and actuating the mechanism. While smart materials have been integrated into certain mechanisms, such integration is generally considered a unique design for specific cases and lacks universality. Therefore, organically combining universal mechanism design with smart materials and 4D printing technology, innovating mechanism types, and systematically exploring the interplay between structural design and morphing control remains an open research area. In this work, a novel form-controlled planar folding mechanism is proposed, which seamlessly integrates the control and actuation system with the structural components and kinematic pairs based on the combination of universal mechanism design with smart materials and 4D printing technology, while achieving self-controlled dimensional ratio adjustment under a predetermined thermal excitation. The design characteristics of the mechanism are analyzed, and the required structural design parameters for the preprogrammed design are derived using a kinematic model. Using smart materials and 4D printing technology, folding programs based on material properties and control programs based on manufacturing parameters are encoded into the form-controlled rod to achieve the preprogrammed design of the mechanism. Finally, two sets of prototype mechanisms are printed to validate the feasibility of the design, the effectiveness of the morphing control programs, and the accuracy of the theoretical analysis. This mechanism not only promotes innovation in mechanism design methods but also shows exceptional promise in satellite calibration devices and spacecraft walking systems.

Keywords Form-controlled mechanism, Self-folding, Smart materials, 4D printing, Morphing control

1 Introduction

Aerospace is critical to China's long-term science and technology development plan [1–4]. Due to space constraints in the launch vehicle cargo bay, mechanisms such as satellite antennas, radar calibration, and spacecraft walking must have a small loading size inside the launch vehicle. In addition, these mechanisms must be reconfigured into a practical working form after delivery to their intended orbit [5–8]. Considering the high-reliability requirements of the space environment, it is necessary to minimize the number of kinematic pairs and drive structures while ensuring adequate functional complexity. Many researchers have attempted to address these challenges. Li et al. [9] designed a spherical radar calibration mechanism based on a positive prism expandable unit, which can

*Correspondence:
Duanling Li
liduanling@126.com
[1] College of Mechanical and Electrical Engineering, Shaanxi University of Science and Technology, Shaanxi 710021, China
[2] School of Automation, Beijing University of Posts and Telecommunications, Beijing 100876, China

achieve approximately tenfold contraction, a maximum unfolded diameter of 10 m, and a small weight while saving a significant amount of installation space. Chen et al. [10] developed a new thick plate folding and spreading mechanism that can be used to widely fold various space engineering structures, such as solar panels. These conventional mechanisms have produced exciting results in practical applications, but none of them fully addresses the challenges of excessive kinematic pairs, complex drives, and insufficient reliability.

To address the above challenges, smart materials and 4D printing technology, with their self-assembling, multifunctional, and programmable features, offer a new design idea. Lan et al. [11] conducted the design, development, and ground-based testing of a deployable shape-memory polymer composite flexible solar array system and then validated it in orbit. Liu et al. [12] investigated the design, properties, and applications of a smart hinge based on shape memory polymer composites. While smart materials have already been incorporated into some mechanisms, such integration is generally considered to be a unique case of design that lacks universality [13]. Therefore, organically combining universal mechanism design with smart materials and 4D printing technology, innovating mechanism types, and systematically exploring the interplay between structural design and morphing control remains an open research area.

In this work, we propose a form-controlled planar folding mechanism (FCPFM), which is derived in previous research on expandable mechanisms [14–16], metamorphic mechanisms [17, 18], reconfigurable mechanisms [19–21], and 4D printing [22]. Meanwhile, high-quality research on angulated scissor units, constraints, and kinematic analysis is also referenced [23–25]. The FCPFM has a novel characteristic, which is not available in the conventional mechanisms, while effectively avoiding the drawbacks associated with the conventional mechanisms. Figure 1 shows the contents of this work, and the main contributions are listed below.

(1) Based on the combination of universal mechanism design with smart materials and 4D printing technology, an FCPFM consisting of an angulated scissor rod (ASR) and a form-controlled rod (FCR) is proposed. The FCPFM enables self-controlled dimensional ratio adjustment under a predetermined thermal excitation.
(2) The construction method of the FCPFM and the kinematic characteristic are analyzed. The critical structural design parameters required for the preprogrammed design are derived based on the kinematic model.

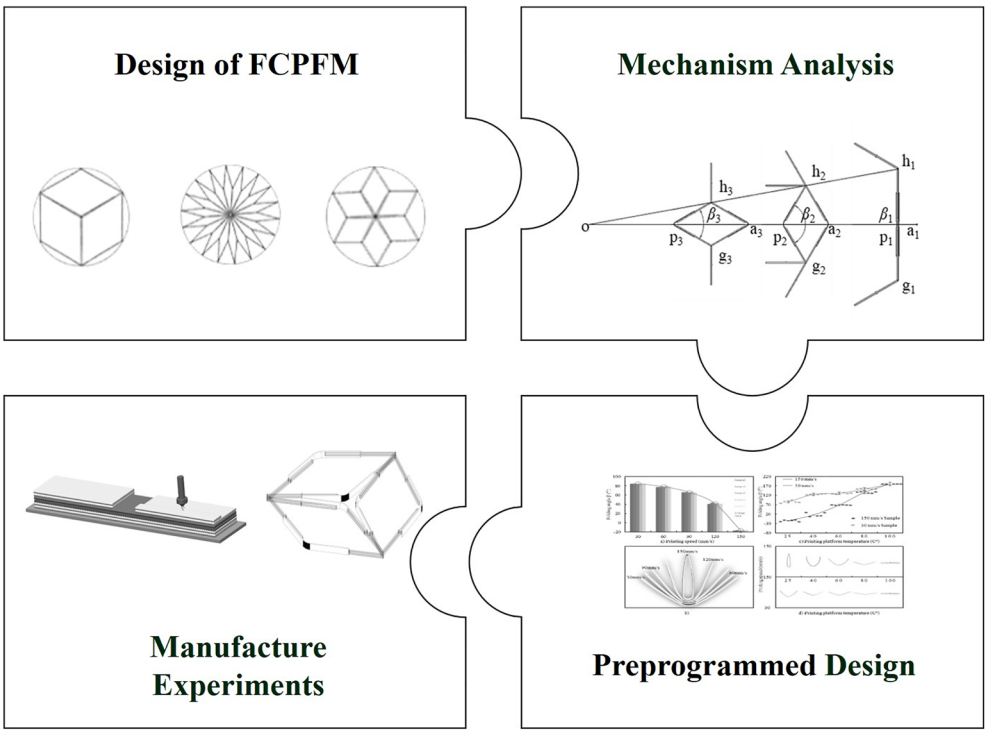

Figure 1 Schematic of work contents

(3) Using smart materials and 4D printing technology, folding programs based on material properties and control programs based on manufacturing parameters are encoded into the form-controlled rod to achieve the preprogrammed design of the FCPFM.
(4) Two sets of prototype FCPFMs are printed and used to verify the feasibility of the design, morphing control programs, and correctness of the theoretical analysis.

2 Design of FCPFM

This section consists of three subsections. First, the design concept of the FCPFM is overviewed. Second, the construction method of the FCPFM and the kinematic characteristics are analyzed. Finally, the kinematic model of the FCPFM is derived.

2.1 Design Concept

This work proposes an FCPFM with thermally excited morphing response characteristics, as shown in Figure 2. The FCPFM maintains an unfolded state at ambient temperature, and the radius of the unfolded circumcircle reaches its maximum value. When the predetermined thermal excitation is applied, the FCPFM folds, and the radius of the folded circumcircle reaches its minimum value.

The ASRs and FCRs constitute the FCPFM, as shown in Figure 2. The ASR controls the construction and folding ratios of the FCPFM based on a designed structure and geometric arrangement. The FCR enables the FCPFM to achieve thermally excited morphing response characteristics.

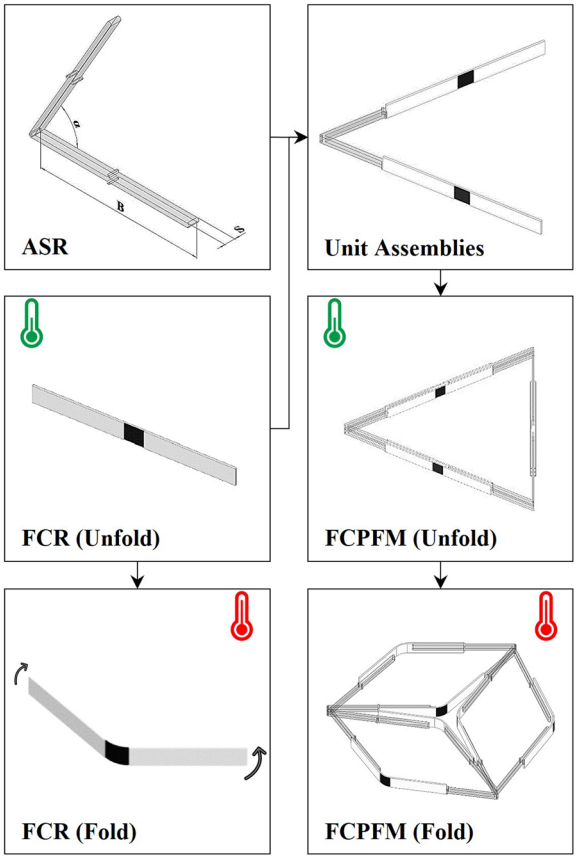

Figure 2 Schematic of FCPFM

2.2 Construction Method and Kinematic Characteristics

The four ASRs (including *dhp*, *bha*, *agc*, and *vgp*) and two FCRs (including *tpz* and *uaj*) are extracted from the FCPFM to create a rectangular coordinate system, as shown in Figure 3a and b. The triangles *hdb* and *hap* are congruent isosceles triangles, with perpendicular lines drawn through point *h* to line *db* and the *x*-axis, intersecting at points *n* and *k*. In combination with Figure 2, the following proof can be made.

Given that, $dh = bh = hp = ha$.

The lines *nh* and *kh* are the perpendicular bisectors of the triangles *dhb* and *ahp*, and it follows that,

$\triangle dhn \cong \triangle bhn \cong \triangle ahk \cong \triangle phk$.

Therefore,

$\angle dhn = \angle bhn = \angle ahk = \angle phk$.

Because the $\angle bhp$ is the common angle, it is evident that,

$2\angle dhn + \angle bhp = 2\angle phk + \angle bhp = \alpha$.

Furthermore, given that,

$\angle dhp = \angle bha = \alpha$, it follows that,

$\angle dhn + \angle bhp + \angle phk = \alpha$.

Furthermore, since,

$\angle ohn = \angle ohk = \pi/2$, it can be concluded that,

$\angle nok = \angle doa = \pi - \alpha$.

Let *m* be the number of the unit groups (*m* contains 2*m* FCRs and 2*m* ASRs) required to construct the FCPFM, and it follows that,

$\angle nok = \angle doa = 2\pi/m$.

We know that,

$$\alpha = \pi - \frac{2\pi}{m} \wedge (m = k + 3 \wedge k \in Z). \tag{1}$$

Based on the proof, it can be concluded that the angle of the circumcircle (such as angle *doa*) corresponding to each group of ASRs remains constant. Therefore, the FCPFM is constructed using *m* groups of units.

The specific construction method is shown in Figures 2 and 3. Hinges connect the ASRs at the *h* and *g*, while the FCRs are bonded at the boundary blocks *t*, *z*, *u*, and *j*. The primary function of the boundary blocks is to prevent uneven force or collision interference between the FCRs and the ASRs due to inaccurate

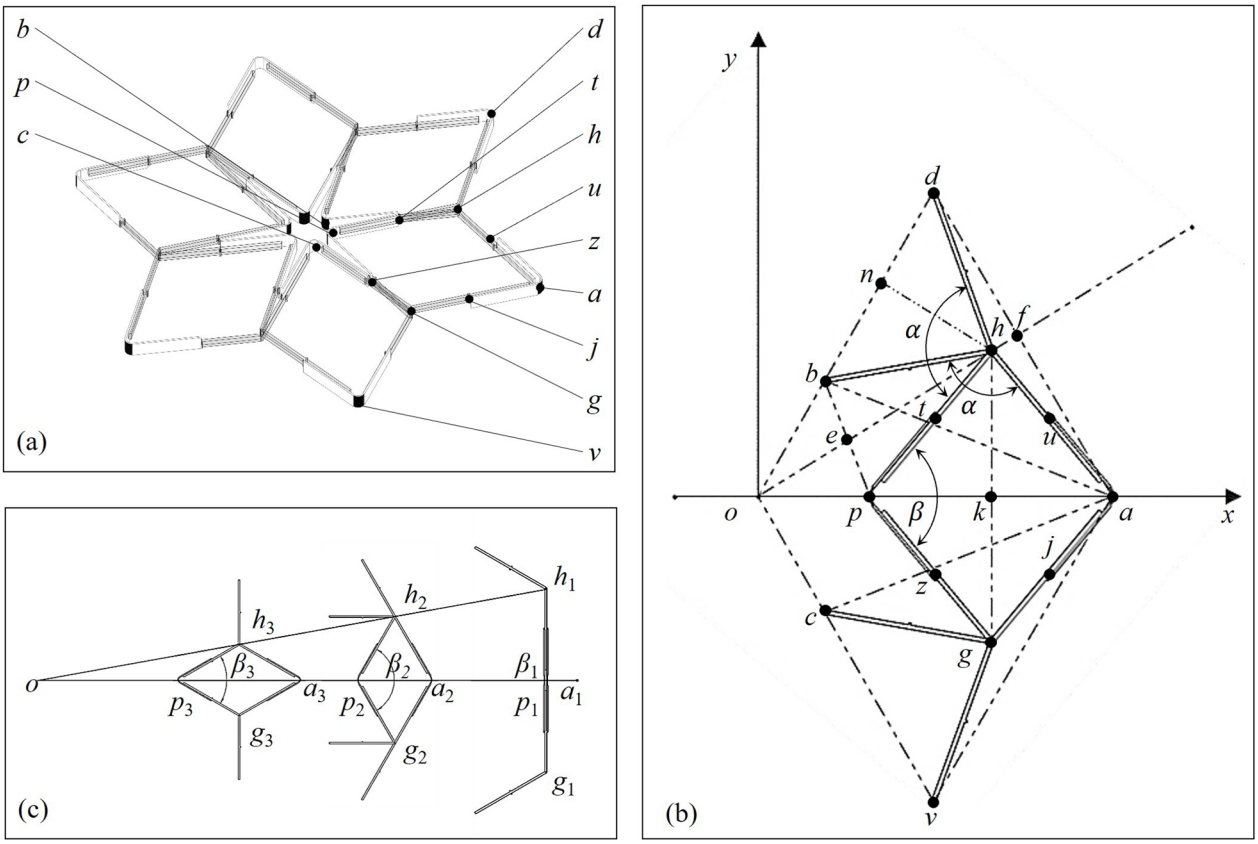

Figure 3 Schematic of FCPFM coordinates: **a** Model coordinates, **b** Coordinate systems of ASR and FCR, **c** Movement process of ASR and FCR

positioning. By analogy, the FCPFM is constructed using m groups of units. Table 1 shows the FCPFMs constructed based on different m.

In this part, the kinematic characteristics of the FCPFM with different m are further discussed. To explain the kinematic characteristics, it is necessary to identify the characteristics of the degrees of freedom of the FCPFM. The ASR is driven by the FCR, which is assumed to extend at both ends and achieve movement through facial contact. Thus, the FCR can be considered to be a planar rotating pair. The FCPFMs constructed with different m are cut along the midpoint of any pair of FCRs and extended into planar kinetic chains, as shown in Table 1.

Applying the loop connectivity matrix (LCM), it is known that,

$$F_{\mathrm{LCM}} = \begin{vmatrix} 1\,1\,0\,0\,0 \\ 0\,1\,1\,0\,0 \\ 0\,0\,1\,1\,0 \\ \\ 0\,0\,0\,\ddots\,1 \\ 0\,0\,0\,0\,m \end{vmatrix}. \tag{2}$$

Table 1 Construction of FCPFM based on different m

m	Planar kinetic chain	Folded	Unfolded
3		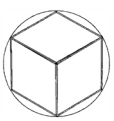	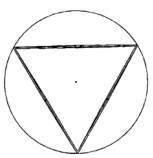
4		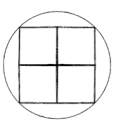	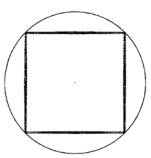
6	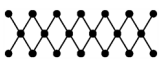		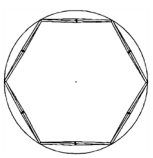
18			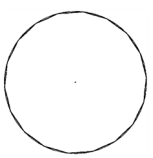

Let $\boldsymbol{F}_{\mathrm{LCM}}$ be the degrees of freedom. Based on the above LCMs, it can be deduced that all FCPFMs are single degrees of freedom.

The kinematic characteristics of the FCPFM are discussed next. From the micro perspective of the ASR and FCR, as shown in Figure 3c, the FCR folds under predetermined thermal excitation, and the self-folding angle change process is β_1 to β_2 to β_3. The midpoint of the FCR, p and a, moves along the connecting line ***ao*** direction, which drives the ASR between the hinge point h along the connecting line ***ho*** direction. Throughout the process, the change in diagonal pa causes the FCPFM to generate planar folding. From the macro perspective of the FCPFM, the abovementioned process transforms an unfolded circumcircle around the center of the FCPFM into a folded circumcircle under a predetermined thermal excitation. As shown in Figure 3c and Table 1, the unfolded circumcircle is formed by connecting a series of diagonal endpoints h in the unfolded state of the FCPFM. The folded circumcircle is formed by connecting a series of diagonal endpoints a in the folded state of the FCPFM.

2.3 Kinematic Model

Let the length of lines dh, bh, ph, and ah be B, as shown in Figure 3b and Figure 2.

First, the kinematic model of a folded circumcircle during the movement of the FCPFM is derived,

The length of the line ad is,

$$ad = 2B\sin\frac{\angle ahd}{2} = 2B\sin(\frac{\pi}{m}+\frac{\beta}{2}). \tag{3}$$

For the triangle doa, we know that,

$$ad^2 = od + oa - 2od\cdot oa\cdot\cos\angle aod. \tag{4}$$

In the triangle doa, od is equal to oa, bringing Eq. (4), we know that,

$$ad^2 = 2oa^2(1-\cos\angle aod) = 4oa^2\sin^2(\frac{\pi}{\mathrm{m}}). \tag{5}$$

Let Eq. (3) be equal to Eq. (5), we can give a kinematic model of the folded circumcircle during the movement of the FCPFM,

$$oa(\beta) = B\sin(\frac{\pi}{\mathrm{m}}+\frac{\beta}{2})\sin^{-1}(\frac{\pi}{\mathrm{m}}). \tag{6}$$

When the self-folding angle reaches a minimum value, the FCPFM is folded. Let $R_{\min}$ be the minimum radius of the folded circumcircle. Let β_3 be the minimum self-folding angle. It is evident that $R_{\min}$ is equal to oa, bringing Eq. (6), we know that,

$$\beta_3 = 2\arcsin(\frac{\boldsymbol{R}_{\min}}{B}\sin\frac{\pi}{m}) - \frac{2\pi}{m}. \tag{7}$$

Additionally, it is evident that,

$$\cos(\frac{2\pi}{m}) = \frac{R_{\min}}{B}. \tag{8}$$

Combining Eq. (8) and Eq. (7), we get,

$$\beta_3 = 2\arcsin(\sin\frac{2\pi}{m}) - \frac{2\pi}{m} = \frac{2\pi}{m}. \tag{9}$$

Second, the kinematic model of an unfolded circumcircle during the movement of the FCPFM is derived.

The length of the line oh is,

$$oh = of - hf = \frac{ad}{2}\cot(\frac{\angle aof}{2}) - B\cos(\frac{\angle aof}{2}+\frac{\beta}{2}). \tag{10}$$

Combining Eq. (4) and Eq. (10), we get a kinematic model of the unfolded circumcircle during the movement of the FCPFM,

$$oh(\beta) = B\cot(\frac{\pi}{m})\sin(\frac{\pi}{m}+\frac{\beta}{2}) - B\cos(\frac{\pi}{m}+\frac{\beta}{2}). \tag{11}$$

When the self-folding angle reaches a maximum value, the FCPFM is unfolded. Let $R_{\max}$ be the maximum radius of the unfolded circumcircle. Let β_1 be the maximum self-folding angle. It is evident that $R_{\max}$ is equal to oh, bringing Eq. (12), we know that,

$$\beta_1 = \arcsin(R_{\max}\sin\frac{\pi}{m}B^{-1}). \tag{12}$$

Additionally, it is evident that,

$$\sin(\frac{\pi}{m}) = \frac{B}{R_{\max}}. \tag{13}$$

From Eq. (13), we can derive,

$$\beta_1 = 2\arcsin(1) = 2\pi \tag{14}$$

Based on the proof and calculations, it can be concluded that m is a critical structural design parameter in controlling the construction and folding ratio of the FCPFM and its morphing. Consequently, the ASR can regulate the construction and folding ratio of the FCPFM by adopting a geometric arrangement based on a predetermined m. However, the single ASR focusing on a geometric feature and topology is insufficient for the design of the FCPFM. Therefore, the design of the FCPFM should first consider the construction method and kinematic characteristics based on the ASR. Then the FCR is preprogrammed to achieve the self-controlled

adjustment of the dimensional ratio of the FCPFM under a predetermined thermal excitation.

3 Preprogrammed Design of FCPFM

This section consists of three subsections. First, the thermodynamic properties of the materials required to print the FCR are characterized. Second, the folding programs of the FCR are encoded by manipulating the distribution and geometry of smart and non-smart materials using 4D printing technology according to the designs of the FCPFM and the characterization of the thermodynamic properties of the materials. Finally, the control programs of the FCR are encoded based on the adjustment of manufacturing parameters to achieve the self-controlled adjustment of the dimensional ratio of the FCPFM under predetermined thermal excitation.

3.1 Characterization of Material Properties

The thermodynamic properties of different materials can be used to encode morphing and control programs within the FCR. In addition, this work uses thermal excitation as a method to activate the FCR. Therefore, material property tests are used to characterize the thermodynamic properties of the materials, which can provide a relevant basis for subsequent research.

Four elastomeric non-smart materials, thermoplastic polyurethane (TPU) (eSUN, Shenzhen, China) (Dake, Shenzhen, China) and one polymeric smart material, polylactic acid (PLA) (Raise, Shanghai, China), are candidates for FCR printing. A dynamic thermomechanical analyzer (DMA-Q800, New Castle, United States) is used to evaluate the dynamic thermomechanical properties of the above materials. The tested filament length is 10 mm, and its diameter is 1.75 mm, with a loading temperature range of 25 to 90 °C. During the test, the temperature is controlled to an accuracy of +/− 0.2 °C at a rate of 2 °C/min while a dynamic axial strain rate of 1 Hz is applied with the tensile mode selected.

As shown in Figure 4, the dynamic thermomechanical analyzer (DMA) test results include the changes in storage modulus (G) and dissipation factor angle (tan δ) with temperature (T). The T_i, T_g, and T_h of PLA are 61.96, 68.02, and 73.52 °C, respectively. The G for PLA corresponding to the three temperatures are 2449.81, 1375.29, and 637.75 MPa, respectively. The T_i, T_g, and T_h represent the beginning, transition, and end temperatures of the glass transition phase of PLA, respectively. Similarly, the DMA test results for TPU show that the T_g of TPU is below ambient temperature, and the G of TPU decreases slowly with increasing temperature.

3.2 Folding Programs

This subsection describes use of 4D printing technology to manipulate the distribution and geometry of smart and non-smart materials to encode the folding programs of the FCR, which enables FCPFM to obtain thermally excited morphing response characteristics to control its structural self-folding.

Using fused deposition modeling (FDM) to manipulate the distribution and geometry of PLA and TPU to encode the folding programs of the FCR, as shown in Figure 5. This structure consists of six layers, four of which are continuous and two of which are split. The split layers are used to control the width of the morphing and compensate for edge bending.

First, the principle of how the folding programs create drive is explained, where the PLA is heated and squeezed during the printing process, causing stretching and alignment of the polymer chains in that direction and subsequent generation of strain. These strains are stored in the printed material due to the constraining effect of the printing platform or previous layer and are fixed layer

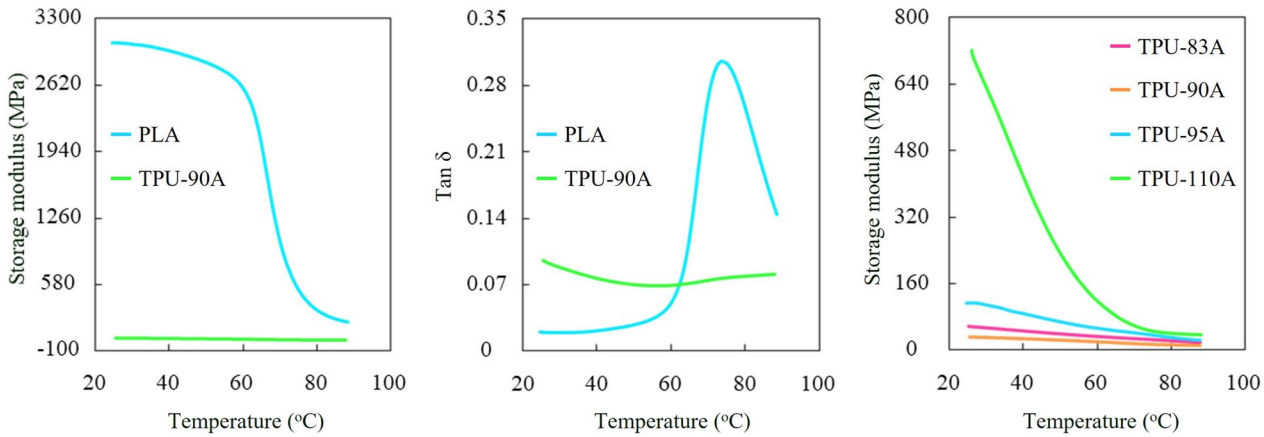

Figure 4 DMA test results, storage modulus and dielectric loss angle of PLA, and storage modulus of TPU

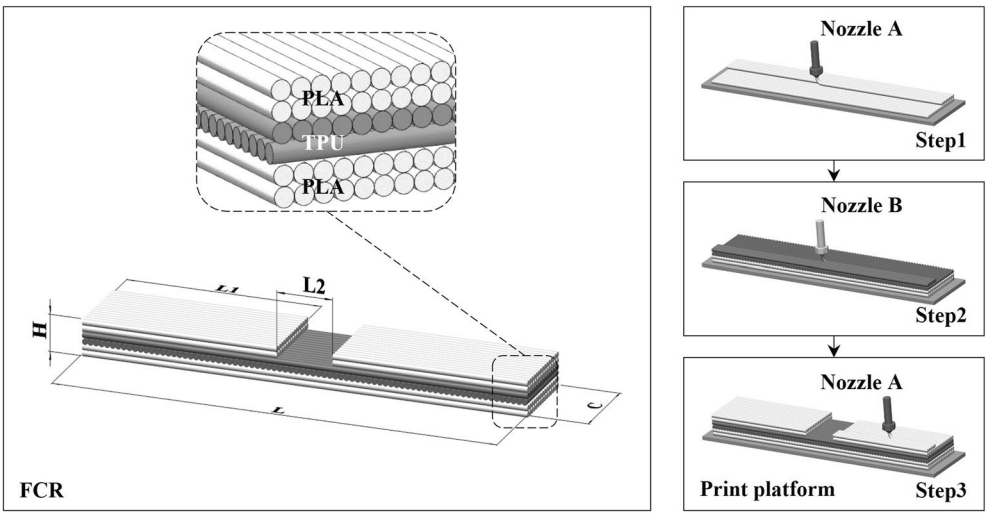

Figure 5 Schematic of FCR

by layer as the printing process cools. When the PLA is removed from the printing platform and reheated above its T_g, the PLA shortens along the print direction and expands slightly in the other two directions.

Second, how to manipulate the distribution and geometry of PLA and TPU for encoding the FCR folding program is explained. PLA with unidirectional fill patterns exhibits anisotropic morphing behavior, which is superior to multidirectional fill patterns [26, 27]. For this reason, in this work, all PLA is printed in the same orientation in the FCR. However, it is difficult to accurately control the deformation of the FCR with monolayer PLA [28]. As shown in Figure 4, the DMA test revealed that the glass transition temperature of TPU is generally lower than the ambient temperature, and the Young's modulus remains relatively constant over the T_h temperature range from ambient temperature to PLA. Therefore, TPU shows relative physical stability in the above temperature range with negligible volume change. The combination of PLA and TPU in the FCR allows TPU to program the uncontrollable morphing of monolayer PLA into controllable self-folding.

3.3 Control Programs

The different m determines the different constructions of the FCPFM, and the variation range of the self-folding angle of the FCR varies depending on the construction. Therefore, in this subsection, the control programs based on the adjustment of manufacturing parameters is discussed. This is encoded to control the variation range of the self-folding angle of the FCR, which realizes the self-controlled adjustment of the dimensional ratio of the FCPFM under predetermined thermal excitation.

First, the control program encoding based on the restrictive capability of TPU is discussed. Four FCRs are printed and tested using a fused deposition modeling printer (Raise E2, Shanghai, China). Hot water is chosen as the activation medium of the experiment to ensure uniform, accurate, and rapid heating [29]. The T_g of PLA is selected from Figure 4. The temperature setting of the heater (LICHEN-HH4, Shanghai, China) is kept constant. All the FCRs are kept in water, and heating is stopped when they show no visual signs of morphing. The printing parameters, structural dimensions, and experimental parameters are shown in Table 2, and the schematic diagram of the structural dimensions is shown in Figure 5.

As shown in Figure 4, when the loading temperature exceeds 25 °C, the storage modulus of the four TPUs gradually decreases with the increase in temperature. Combined with the experiments, it is found that, the more storage modulus of TPU, the better is the resilience. Therefore, the stronger the resistance of TPU's resistance against the shortening of PLA is, the smaller is the variation range of the self-folding angle, as shown in Figure 6. In summary, the storage modulus of TPU can be used to control the variation range of the self-folding angle.

It is imperative to note that the control of morphing using the restrictive capability of TPU depends on the inherent properties of TPU. The modification of TPU involved physical mixing, chemical chain expansion, grafting, and crosslinking of polymers due to its complexity and lack of systematic and regular properties. Therefore, in this work, this mode is not selected to control the variation range of the self-folding angle of the FCR. According to another experimental result in the literature [30], the lower the percentage of hard polymer segments

Table 2 Experimental parameters of TPU restricting FCR

Structural dimensions (mm)	***H***	***C***	L_1	L_2	***L***
	1.2	**10**	**45**	**10**	**100**
Printing parameters	Platform temperature (°C)			25	
	Printing speed (mm/s)			PLA 30/TPU 30	
	Layer height (mm)			0.2	
	Infill amount			100%	
	Extrusion width (mm)			0.4	
	Nozzle diameter (mm)			0.4	
	Printing temperature (°C)			PLA 235/TPU 215	
Experimental parameters	Activation medium			Water	
	Activation temperature (°C)			68	
	Water bath time (min)			≤3	

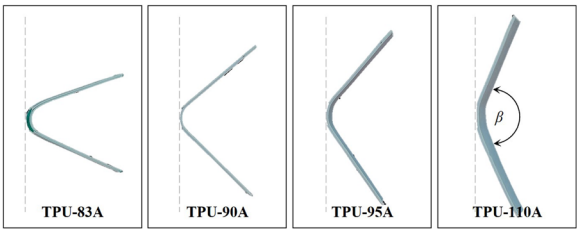

Figure 6 Experimental results of TPU restricting FCR

supporting TPU, the more difficult it is to print. In this work, a single TPU-90A (eSUN, Shenzhen, China) is selected for printing the FCR after considering the printing quality and material properties.

Second, the control program encoding based on the strain storage capability of PLA is discussed. On the one hand, adjusting the printing speed causes different stretching of the PLA during the extrusion process, resulting in different strains stored in the FCR. On the other hand, adjusting the temperature of the printing platform causes different mobility of the polymer chains in the PLA, resulting in different fixation times of their macroscopic shapes and strain relaxation effects, which also causes a difference in the strain stored in the FCR. Therefore, the strain stored in the PLA can be controlled by experimentally adjusting the printing speed parameter or the temperature parameter of the printing platform. These two modes can control the variation range of the self-folding angle.

For a more accurate and quantitative evaluation of the experimental results, a 3D optical scanner (MetraSCAN 3D, Lévis, Canada) is used to measure the self-folding angle after the experiment, as shown in Figure 7. The FCRs are cooled to ambient temperature by removing them from a constant temperature water bath, which is followed by placing them on a scanning test bench for scanning. The data obtained is used to synthesize a 3D model for later quantitative morphing evaluation.

The experiments are set up to investigate the temperature parameter of the printing platform that control the self-folding angle of the FCR. The first group of 25 FCRs is equally divided into five teams and printed with the printing platform temperature set to 25 °C, 40 °C, 60 °C, 80 °C, and 100 °C and the PLA printing speed set to 150 mm/s. The second group of 25 FCRs is equally divided into five teams and printed with the same platform temperature setting as the first group, and the PLA print

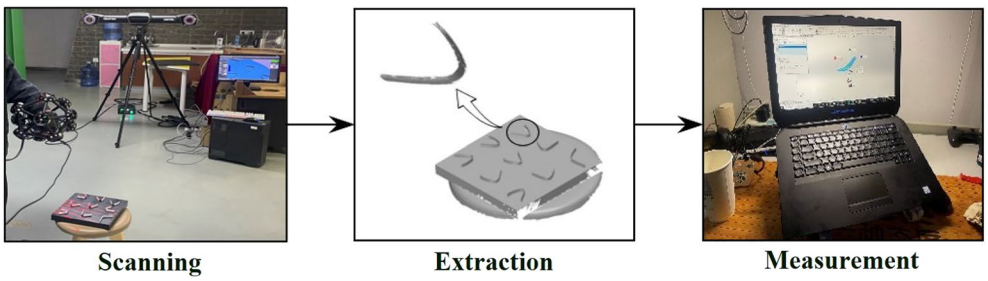

Figure 7 3D optical scanning processes

speed is set to 30 mm/s. The other parameters are the same as those shown in Table 2, except for the above control parameters. The measured results of the self-folding angle in the experiment of adjusting the temperature parameters of the printing platform are shown in Figure 8a and b. The experimental results are as follows.

(1) Printing PLA on the lower-temperature printing platform can quickly fix the polymer chains in a stretched state, which helps to maintain a higher strain and thus a wider range of self-folding angle variation. Therefore, the variation range of the self-folding angle of the FCR can be controlled by the temperature parameter of the printing platform, provided that the printing speed of the PLA is kept constant.
(2) The printing speed of the PLA can control the variation range of the self-folding angle of the FCR.
(3) Compared to the average value, the self-folding angle of FCR is unstable at different temperatures. This is because the temperature of the printing platform controls the range of variation of the self-folding angle, mainly in the first layer, which is affected and gradually normalized in the subsequent layers. Therefore, the success of this control depends on the entire printing structure being at a constant temperature. A closed chamber is used in the experiments, but because there is no thermostat, the experimental results still show that the FCR is affected by the external ambient temperature.

The experiments are set up to investigate the printing speed parameters that control the self-folding angle of the FCR. The group of 25 FCRs is divided equally into five teams and printed with the PLA printing speed set to 30 mm/s, 60 mm/s, 90 mm/s, 120 mm/s, and 150 mm/s, and the printing platform temperature is set to 25°C, which is the same as that of the ambient temperature. The other parameters are the same as those shown in Table 2, except for the above control parameters. The measured results of the self-folding angle in the printing speed parameter adjustment experiment are shown in Figure 8c and d. The experimental results are as follows.

(1) Printing PLA at higher printing speeds allows greater stretching of the polymer chains during the

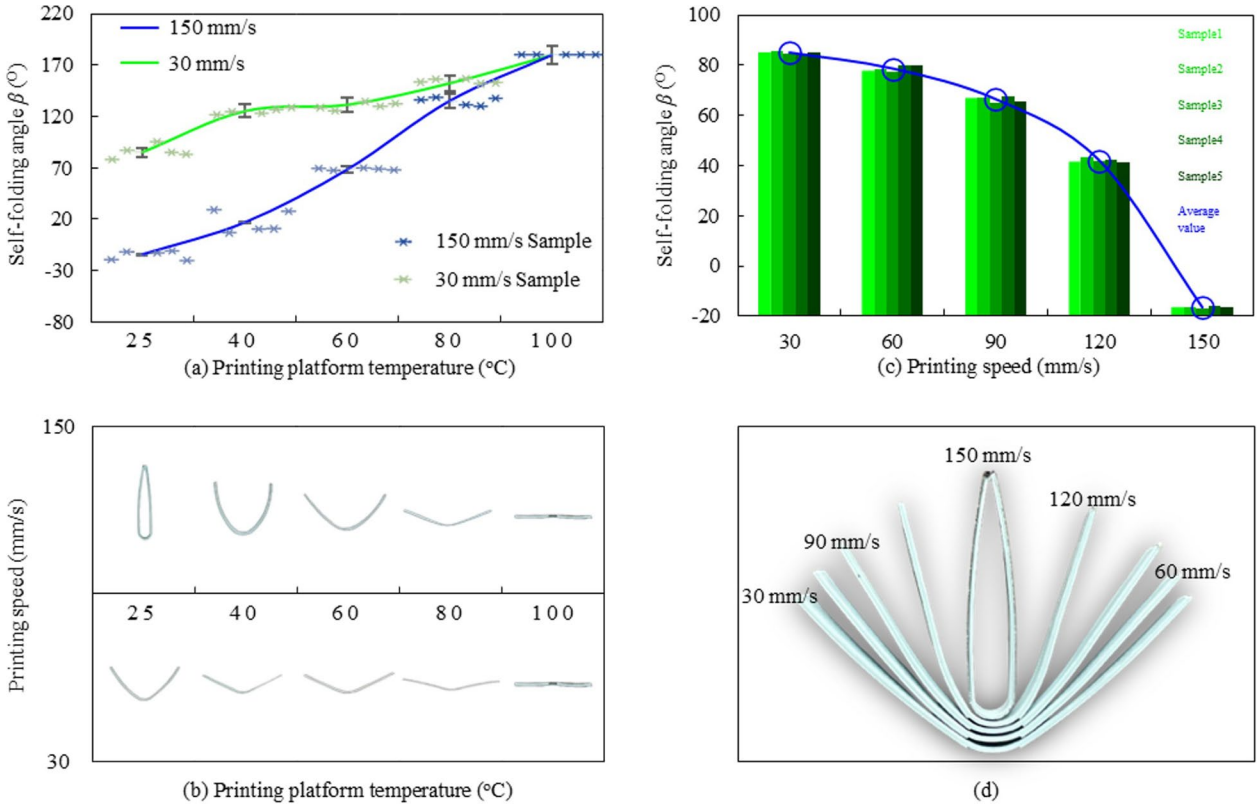

Figure 8 Experiment of the self-folding angle control based on manufacturing parameters: **a** Self-folding angle control based on printing platform temperature, **b** FCRs after morphing caused by printing platform temperature, **c** Self-folding angle control based on printing speed, **d** FCRs after morphing caused by printing speed

extrusion process, which helps to maintain higher strains and thus a wider range of self-folding angle variations. Therefore, the variation range of the self-folding angle of the FCR can be controlled by the printing speed parameter of the PLA, provided that the temperature of the printing platform is kept constant.

(2) Compared with the previous experimental group, the self-folding angle of FCR is relatively stable at different printing speeds. On the one hand, the printing of the FCRs is less affected by the external ambient temperature. On the other hand, the stepper motor controls the printing speed almost independently of the external ambient temperature and is precisely controlled. As a result, the print speed parameter is more accurate and easier in terms of controlling the variation range of the self-folding angle of the FCR compared to the temperature parameter of the printing platform.

4 Experiments of FCPFM

This section consists of two subsections. First, two FCPFMs are printed with the m taken as 3 and 6, named M3 and M6, respectively. Second, the correctness of the mechanism design and analysis and the feasibility of the morphing control programs are experimentally verified.

The dual nozzle printer is used for rapid prototyping in the FCPFM. The M3 consists of 6 ASRs and 6 FCRs. The M6 consists of 12 ASRs and 12 FCRs. The ASR is printed using a common high-temperature-resistant polycarbonate material (Raise, Shanghai, China). First, the side length B of the ASR is determined. Then, the top angle α of the ASR is determined from Eq. (1) based on the m. Due to the limitation of thickness K, the FCPFM does not reach the theoretical state. Therefore, the theoretically calculated radius of the unfolded and folded circumcircle is slightly smaller or larger than the actual values. The specific manufacturing parameters are shown in Table 3.

It is crucial to describe the printing process of the FCR because it includes the necessary control and folding of the FCPFMs. The variation range of the self-folding angle of different mechanisms is calculated by Eq. (9) and Eq. (14) based on m. According to the calculation results, it is necessary to select the control programs given in subsect. 3.2 of this work based on the printing equipment, test conditions, and practical situation. Using the selected control programs, the variation curve of the self-folding angle is obtained. Finally, based on this curve, the fiducial printing speed or fiducial temperature of the printing platform is found. Select control parameters that are below the fiducial temperature or above the fiducial speed to complete printing. In this work, to ensure the comprehensive validation effect of the FCPFM, the M3 adopts the temperature parameter of the printing platform to control the self-folding angle of the FCR. The M6 adopts the printing speed parameter to control the self-folding angle of the FCR. The specific printing and control parameters are shown in Table 4.

M3 and M6 are printed according to the above parameters. The experimental result is shown in Figure 9, and the experimental verification conditions and parameter settings are consistent with the previous experiments. In the state of no thermal excitation, the FCR is flat, the self-folding angle is at its maximum, and the FCPFM is unfolded. The radius of the unfolded circumference of M3 and M6 are 102.92 mm and 129.26 mm, respectively. When a predetermined thermal excitation is applied, the FCR undergoes a controllable morphing from a flat state to a self-folded state. The self-folding angle is at the set value, which is the minimum value. The FCPFM is folded, and the radius of the folded circumference of M3 and M6 are 93.69 mm and 115.23 mm, respectively.

The experimental results show that the FCPFM can realize the self-controlled adjustment of the dimensional ratio under the predetermined thermal excitation according to the preprogrammed design.

Table 3 Manufacturing parameters of ASR

Number of unit groups m	Top angle α (°)	Theoretical circumcircle radius		Theoretical rod length B (mm)	Thickness K (mm)	Width S (mm)
		R_{min} (mm)	R_{max} (mm)			
3	60°	90	103.92	90	3	5
6	120°	112.58	130	65	3	5

Printing platform temperature (°C)	Printing speed (mm/s)	Layer height (mm)	Infill amount	Extrusion width (mm)	Printing temperature (°C)
110	60	0.2	15%	0.4	235

Table 4 Manufacturing and control parameters of FCR

Height H (mm)	Width C (mm)	Separate layer width L_1 (mm)	Separate layer spacing distance L_2 (mm)	Length L (mm)
1.2	10	45	10	100

Number of unit groups m	Folding angle range β (°)	Self-folding angle control method	PLA printing speed		TPU printing speed (mm/s)	Platform temperature	
			Fiducial value (mm/s)	Actual value (mm/s)		Fiducial value (°C)	Actual value (°C)
3	[120°, 180°]	Platform temperature	150		30	75	60
6	[60°, 180°]	Printing speed	100	110	30	25	

5 Conclusions

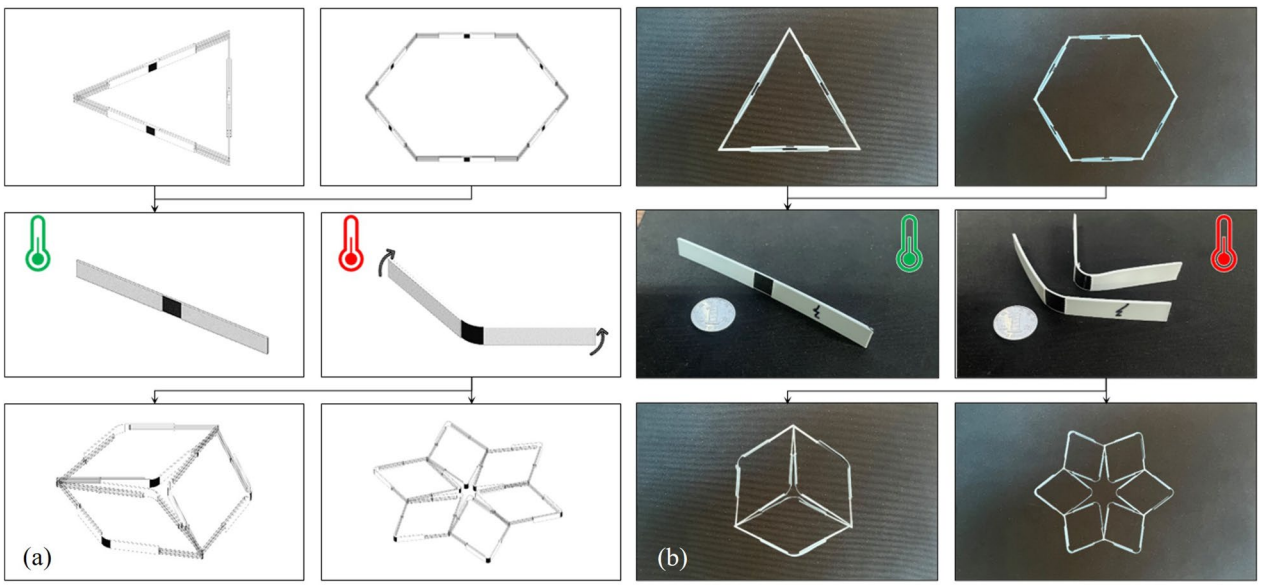

Figure 9 Experiments of FCPFM: (a) Digital models, (b) Prototype machines

(1) In this work, a novel type of mechanism, the FCPFM, is designed. Unlike conventional mechanisms, the FCPFM utilizes 4D printing technology and smart materials to seamlessly integrate the control and actuation system with the structural components and kinematic pairs. This innovative design effectively addresses the problems of excessive kinematic pairs, complex drive mechanisms, and limited reliability encountered in conventional mechanism design. In addition, unlike the manual control methods used in conventional mechanisms, the FCPFM incorporates environmental sensing capabilities. This allows for self-controlled adjustment of the dimensional ratio under predetermined thermal excitation.

(2) This research differs from the unique case application of smart materials in some mechanisms. By incorporating smart materials into the universal mechanism design, systematic research is conducted on a type of mechanism from structural design to morphing control, which promotes the innovation of mechanism design methods.

(3) This design is expected to introduce a new paradigm of 4D printing technology into conventional mechanism design, providing new ideas for aerospace equipment design. For example, the FCPFM can be spatially arranged according to specific geometries and topologies to create form-controlled spatial folding mechanisms for space satellite calibration devices. FCPFMs can also be attached to external structures, such as external hubs, to develop variable-diameter wheels suit-

able for spacecraft walking systems. These potential applications provide a valuable direction for future research efforts.

Acknowledgements
Not applicable.

Author contributions
WZ was in charge of the whole trial; WZ wrote the manuscript; ZG and DL assisted with analyses and experiments. All authors read and approved the final manuscript.

Authors' Information
Wencai Zhang, born in 1989, is currently a Ph.D. candidate in the *College of Mechanical and Electrical Engineering, Shaanxi University of Science and Technology, China*. He received his master's degree from *Fujian Agriculture and Forestry University, China*. Zhang's research interests include 4D printing, mechanisms, and robotics.
Zhenghao Ge, born in 1964, is currently a professor and Ph.D. advisor in the *College of Mechanical and Electrical Engineering, Shaanxi University of Science and Technology, China*. He received his Ph.D. degree from *Xi'an University of Technology, China*. Ge's research interests include robotic mechanisms, automated mechanical systems, and 3D printing systems with multiple materials.
Duanling Li, born in 1974, is currently a professor and Ph.D. advisor in the *School of Automation, Beijing University of Posts and Telecommunications, China*, and a distinguished professor and Ph.D. advisor in the *College of Mechanical and Electrical Engineering at Shaanxi University of Science and Technology, China*. She received her Ph.D. degree from *Beihang University, China*. Li's research interests include robotics and mechanisms.

Funding
Supported by National Natural Science Foundation of China (Grant No. 52175019), Beijing Municipal Natural Science Foundations (Grant Nos. 3212009 and L222038), and Beijing Municipal Key Laboratory of Space-ground Interconnection and Convergence of China.

Data availability
All data and materials generated or analysed during this study are included in this published article.

Declarations

Competing Interests
The authors declare no competing financial interests.

Received: 8 May 2022 Revised: 4 July 2023 Accepted: 9 July 2023
Published online: 01 September 2023

References

[1] G Z Bai, X Y Cao. Thoughts on systematic layout of strengthening national strategic scientific and technological power. *Bulletin of Chinese Academy of Sciences*, 2021, 36(5): 523–532.
[2] H Y Hu, C B Guo. Thinking on CAS supporting development of national aerospace science and technology strength. *Bulletin of Chinese Academy of Sciences*, 2021, 36(Z2): 64–69. (in Chinese)
[3] Y Li, Y Xiao, L Yu, et al. A review on the tooling technologies for composites manufacturing of aerospace structures: materials, structures and processes. *Composites Part A: Applied Science and Manufacturing*, 2022, 154: 106762.
[4] Y R Zhou, Z C Shen, Z Y Qi, et al. Demand for high performance materials in development of China's aerospace science and technology. *Cailiao Gongcheng/Journal of Materials Engineering*, 2021, 49(11): 41–50. (in Chinese)
[5] F W Taylor, B Carpenter, J Hacker, et al. Geostationary small satellite for operationally responsive space (ORS) communications missions. *Space 2008 Conference*. San Diego, California, United States, September 9, 2008: 1–14.
[6] Q Deng, B Li, H L Huang, et al. Design and analysis of a tapered deployable mast. *3rd International Conference on Advanced Design and Manufacture*. Nottingham, United Kingdom, September 08–10, 2011: 31–34.
[7] H P Liu, A Luo, L X Zhang. Analysis of movement and stability of the root lock mechanism of the space deployable mast. *2010 IEEE International Conference on Mechatronics and Automation*. Xi'an, China, August 4–7, 2010: 1175–1178.
[8] H W Guo, R Q Liu, Z Q Deng. Mechanics analysis of beam-like space deployable truss mast. *2011 1st International Conference on High Performance Structures and Materials Engineering*. Beijing, China, June 2-3, 2011: 717–722.
[9] D L Li, K Dong, L Liu, et al. Design method and research of spherical radar calibration mechanism based on positive pyramid expandable unit. *Journal of Mechanical Engineering*, 2020, 56(5): 123–132. (in Chinese)
[10] Y Chen, R Peng, Z You. Origami of thick panels. *Science*, 2015, 349(6246): 396–400.
[11] X Lan, L W Liu, F H Zhang, et al. World's first spaceflight on-orbit demonstration of a flexible solar array system based on shape memory polymer composites. *Science China Technological Sciences*, 2020, 63(8): 1436–1451.
[12] Z X Liu, X Lan, W F Bian, et al. Design, material properties and performances of a smart hinge based on shape memory polymer composites. *Composites Part B: Engineering*, 2020, 193: 108056.
[13] W C Zhang, Z H Ge, D L Li. Evolution and emerging trends of 4D printing: A bibliometric analysis. *Manufacturing Review*, 2022, 9(30): 2022028.
[14] Buckminster Fuller. Tensegrity. *Portfolio and Art News Annual*. 1961, 4: 112–127, 144.
[15] L J Shen, K Di, P H Li, et al. Design and mechanical analysis of cable rod truss deployable mechanism. *Journal of Mechanical Engineering*, 2022, 58(17): 135–143. (in Chinese)
[16] Y E Geints, A V Klimkin, S V Latynsev, et al. Geometrical-optics computer model of metal-knitted mesh for calculations of solar pressure on space deployable antenna reflectors. *Applied Optics*, 2019, 58(14): 3815–3822.
[17] J S Dai, J Rees Jones. Mobility in metamorphic mechanisms of foldable/erectable kinds. *Journal of Mechanical Design*, 1999, 121(3): 375–382.
[18] F J Espinosa-Garcia, R Tapia-Herrera, E Lugo-González, et al. Development of a robotic hand based on a palm with a metamorphic mechanism for extending the thumb's functionality. *Journal of the Brazilian Society of Mechanical Sciences and Engineering*, 2021, 43(8): 4042021.
[19] W Q Liu, H Q Jiang, Y Chen. 3D programmable metamaterials based on reconfigurable mechanism modules. *Advanced Functional Materials*, 2022, 32(9): 2109865.
[20] A Dogra, S Padhee, E Singla. Optimal architecture planning of modules for reconfigurable manipulators. *Robotica*, 2020, 41(1): 16–30.
[21] N Stravopodis, V C Moulianitis. Anatomy categorization of a serial metamorphic manipulator for optimized robust controller performance. *International Conference on Robotics in Alpe-Adria Danube Region 2022*. Klagenfurt Land, Carinthia, Austria, June 8–10, 2022: 229–238.
[22] W C Zhang, D L Li. Shape memory polymer-based prefabricated components: design ideas and prospects. *Frontiers in Materials*, 2023, 10: 1095384.
[23] Z You, S Pellegrino. Foldable bar structures. *International Journal of Solids and Structures*, 1997, 34(15): 1825–1847.
[24] G C Bai, Q Z Liao, D L Li, et al. Synthesis of scaling mechanisms for geometric figures with angulated-straight elements. *Proceedings of the Institution of Mechanical Engineers, Part C: Journal of Mechanical Engineering Science*, 2013, 227(12): 2795–2809.
[25] R M Li, Y A Yao, X W Kong. A class of reconfigurable deployable platonic mechanisms. *Mechanism and Machine Theory*, 2016, 105: 409–427.
[26] L Kačergis, R Mitkus, M Sinapius. Influence of fused deposition modeling process parameters on the transformation of 4D printed morphing structures. *Smart Materials and Structures*, 2019, 28: 105042.
[27] M H Sehhat, A Mahdianikhotbesara, F Yadegari. Verification of stress transformation in anisotropic material additively manufactured by fused deposition modeling (FDM). *International Journal of Advanced Manufacturing Technology*, 2022, 123: 1777–1783.
[28] M Bodaghi, A R Damanpack, W H Liao. Adaptive metamaterials by functionally graded 4D printing. *Materials & Design*, 2017, 135: 26–36.
[29] F F Wang, F X Luo, Y X Huang, et al. 4D printing via multispeed fused deposition modeling. *Advanced Materials Technologies*, 2023, 8(2): 202201382.

[30] D Rahmatabadi, I Ghasemi, M Baniassadi, et al. 3D printing of PLA-TPU with different component ratios: Fracture toughness, mechanical properties, and morphology. *Journal of Materials Research and Technology*, 2022, 21: 3970–3981.